High-spin states and band terminations in ^{69}As

I. Stefanescu,[1,2] J. Eberth,[1] G. Gersch,[1] T. Steinhardt,[1] O. Thelen,[1] N. Warr,[1] D. Weisshaar,[1] B. G. Carlsson,[3] I. Ragnarsson,[3] G. de Angelis,[4] T. Martinez,[4] A. Jungclaus,[5] R. Schwengner,[6] K. P. Lieb,[7] E. A. Stefanova,[7,8] and D. Curien[9]

[1]*Institut für Kernphysik, Universität zu Köln, Zülpicher Strasse 77, D-50937 Köln, Germany*

[2]*Horia-Hulubei National Institute for Physics and Nuclear Engineering, P. O. Box MG-6, Bucharest, Romania*

[3]*Department of Mathematical Physics, Lund Institute of Technology, P. O. Box 118, S-22100 Lund, Sweden*

[4]*Istituto Nazionale di Fisica Nucleare, Laboratori Nazionali di Legnaro, via Romea 4, I-35020 Legnaro, Italy*

[5]*Departamento de Fisica Teórica, Universidad Autonoma de Madrid, E-28049 Madrid, Spain*

[6]*Institut für Kern- und Hadronenphysik, Forschungszentrum Rossendorf, D-01314 Dresden, Germany*

[7]*II Physikalisches Institut, Universität Göttingen, D-37073 Göttingen, Germany*

[8]*Institute for Nuclear Research and Nuclear Energy, BAS, 1784 Sofia, Bulgaria*

[9]*Institut de Recherches Subatomiques, CNRS-IN2P3, F-67037 Strasbourg, France*

(Received 15 June 2004; published 8 October 2004)

Excited levels in ^{69}As were studied using the ^{40}Ca(^{32}S,$3p$)^{69}As reaction at 95 and 105 MeV beam energy. Gamma rays were detected with the EUROBALL spectrometer operated in conjunction with the Neutron Wall and the charged-particle detector array EUCLIDES. New level sequences with positive and negative parity were identified from $3p$-$\gamma\gamma$ and $\gamma\gamma\gamma$ coincidences. Spins were assigned to many of the levels on the basis of directional correlations of oriented states measurements. The previously observed positive-parity band was extended to spin $45/2^+$ and it was found to exhibit a crossing with another configuration identified up to spin $53/2^+$. Three negative-parity bands were observed for the first time up to spins $(43/2^-)$, $39/2^-$, and $(41/2^-)$. The previously known band was extended to spin $(49/2^-)$. No evidence for superdeformation was found, despite very high counting statistics. Configurations were assigned to each of the observed bands through comparisons to the cranked Nilsson-Strutinsky calculations.

DOI: 10.1103/PhysRevC.70.044304 PACS number(s): 23.20.Lv, 21.10.Re, 27.50.+e, 21.60.−n

I. INTRODUCTION

Low-spin structures in odd-As isotopes are known from several investigations employing β-decay studies [1,2], (^{3}He,d) and (p,n) reactions [3,4], or heavy-ion reactions [5–8]. Decoupled rotational bands built on the $g_{9/2}$ orbital have been firmly established and their systematic trends extensively discussed [3,5,7,8]. The low-lying negative-parity structures were found to consist of single-particle states and rotational bands whose properties are mainly determined by the $p_{1/2}$,$p_{3/2}$, and $f_{5/2}$ orbitals.

Although the experimental efforts were mostly concentrated on high-spin studies in the last decade, information about the structure of the odd-As isotopes at high excitation energy is still rather scarce. Positive-parity states above spin $21/2^+$ have been observed so far in ^{67,69,71}As [9–12] whereas high-spin negative-parity bands are firmly identified only in ^{71}As [12,13]. The investigations revealed that the general structures of these nuclei have some features in common, but, with increasing neutron number, important differences occur. For example, the yrast bands in ^{67,69}As were found to exhibit a sharp backbending at $\hbar\omega \approx 0.52$ MeV [9,11], while in ^{71}As no evidence for a band crossing was found up to the highest observed spin of $(29/2^+)$ corresponding to $\hbar\omega \approx 0.65$ MeV [12]. Such differences in the structure of nuclei are probably connected with the competing gaps in the Nilsson single-particle levels for $N=34$, 36, and 38 at prolate or oblate deformations, leading to different nuclear shapes and different behaviors of the yrast line with increasing neutron number.

In this paper we present new comprehensive low- and high-spin data for the nucleus ^{69}As. Prior to this work, positive-parity states up to spin $(41/2^+)$ have been reported in Ref. [11]. High-spin negative-parity states up to spin $25/2^-$ have been observed in the work of Mitarai *et al.* [10] and partially confirmed in [11]. Thus, the present study was aimed at extending the positive-parity structure to higher spin and rigorously identifying the negative-parity states in ^{69}As. Since a low-lying negative-parity band based on the $f_{7/2}$ proton orbital has been identified in ^{71}As [13], we address the question whether such a band exists in ^{69}As.

II. EXPERIMENTAL DETAILS AND DATA ANALYSIS

High-spin states in ^{69}As were populated via the ^{40}Ca(^{32}S,$3p$) reaction at 95 and 105 MeV beam energy delivered by the VIVITRON accelerator of the IReS Strasbourg. In the experiment at 105 MeV, the target consisted of a 860 μg/cm^2 self-supporting foil of ^{40}Ca enriched to 99.965%. In the second experiment, performed at 95 MeV beam energy, a foil of 1 mg/cm^2 of ^{40}Ca enriched to 99.9% evaporated onto a 15 mg/cm^2 gold backing was used. Gamma rays were detected with the EUROBALL array [14,15] consisting of 15 Cluster [16] and 26 Clover [17] composite Ge detectors each surrounded by a bismuth germanate shield providing Compton suppression. Charged particles were detected using the 4π device EUCLIDES [18], composed of 40 ΔE-E silicon telescopes with the five forward elements electrically segmented into four parts. The evaporated neutrons were detected with the Neutron Wall

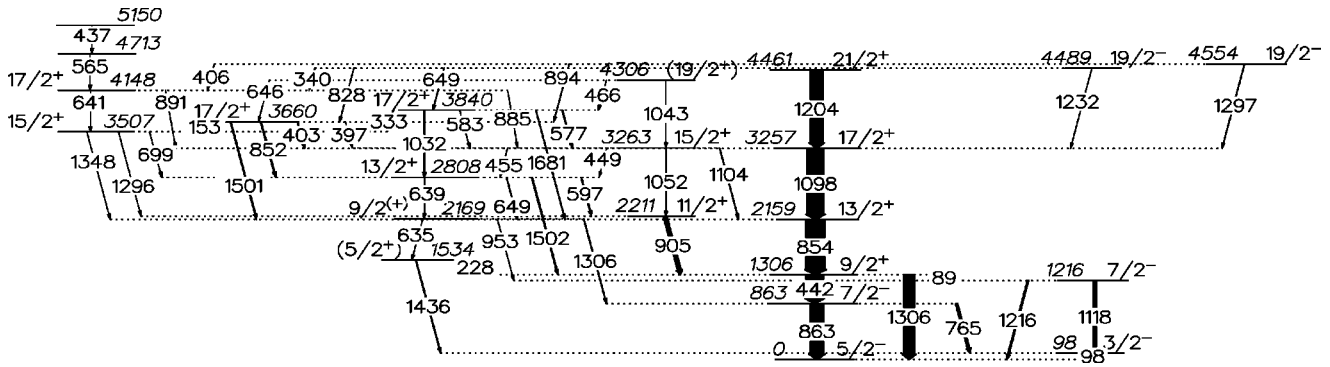

FIG. 1. Low-lying positive-parity states in ^{69}As obtained from the present work. The widths of the arrows are proportional to the γ-ray intensities.

[19], consisting of 50 liquid scintillators covering the forward 1π section of EUROBALL. The events in the experiment at 105 MeV were collected when at least three Ge detectors and one event (neutron or γ) in the Neutron Wall were registered in coincidence. The data from the experiment at 95 MeV were acquired if a minimum of two Ge detectors fired in coincidence with one event in the Neutron Wall.

Data were stored on tapes and sorted off line into E_γ-E_γ matrices and E_γ-E_γ-E_γ cubes, with particle gates on three protons in order to enhance the ^{69}As reaction channel. For energy and efficiency calibrations, ^{152}Eu and ^{56}Co sources were used. A comparison of the peak positions at different detector angles yielded an average velocity of the recoiling nuclei $v/c=2.67\%$. With this value, a Doppler correction of the γ-ray energies was carried out on an event-by-event basis for the data from the self-supporting target experiment. A total number of 8×10^9 $\gamma\gamma\gamma$ events were recorded in the experiment at 105 MeV, whereas in the experiment performed at 95 MeV, the $\gamma\gamma\gamma$ cubes contained about 3×10^9 events. The cubes and the matrices were analyzed using the GASPWARE [20] and RADWARE [21] software packages.

An analysis of the directional correlations from oriented states (DCO's) was performed in order to assign spins to the newly observed states. Since the DCO ratios are very sensitive to the observation angles of the coincident γ rays, specific groups of detectors have to be chosen for the analysis. The geometry of the EUROBALL leads to the formation of 13 rings positioned at angles of 72°, 81°, 99°, 107°, 123°, 129°, 133°, 137°, 141°, 146°, 149°, 156°, and 163°. For the present DCO analysis, the coincidence data were added up for the four most backward-angle rings (163°, 156°, 149°, and 146°), resulting in a quasiring at a weighted average angle of 155° to the beam axis and the four rings near 90° (72°, 81°, 99°, and 107°). A 155° versus 90° γ-γ matrix was created in coincidence with three protons for each experiment. From these matrices, we extracted the DCO ratios defined as [22]

$$R_{DCO}^{expt}=\frac{I^{\gamma 2}_{155^\circ}(\text{gate}^{\gamma 1}_{90^\circ})}{I^{\gamma 2}_{90^\circ}(\text{gate}^{\gamma 1}_{155^\circ})}, \tag{1}$$

where $I^{\gamma 2}_{155^\circ}(\text{gate}^{\gamma 1}_{90^\circ})$ denotes the efficiency-corrected coincidence intensity of the γ_2 transition observed at 155° when gating on the γ_1 transition observed at 90°. In this geometry, if one gates on a stretched quadrupole transition, the theoretical DCO ratios are $\sim$1 for stretched quadrupole transitions and $\sim$0.5 for pure dipole transitions. If, in contrast, gates are set on a pure dipole transition, the extracted DCO ratios are $\sim$2 for pure quadrupole transitions and $\sim$1 for pure dipole transitions.

III. EXPERIMENTAL RESULTS

The ground state spin of $I^\pi=5/2^-$ in ^{69}As has been determined in an atomic-beam nuclear magnetic resonance (NMR) experiment [23]. Low-lying positive-parity states up

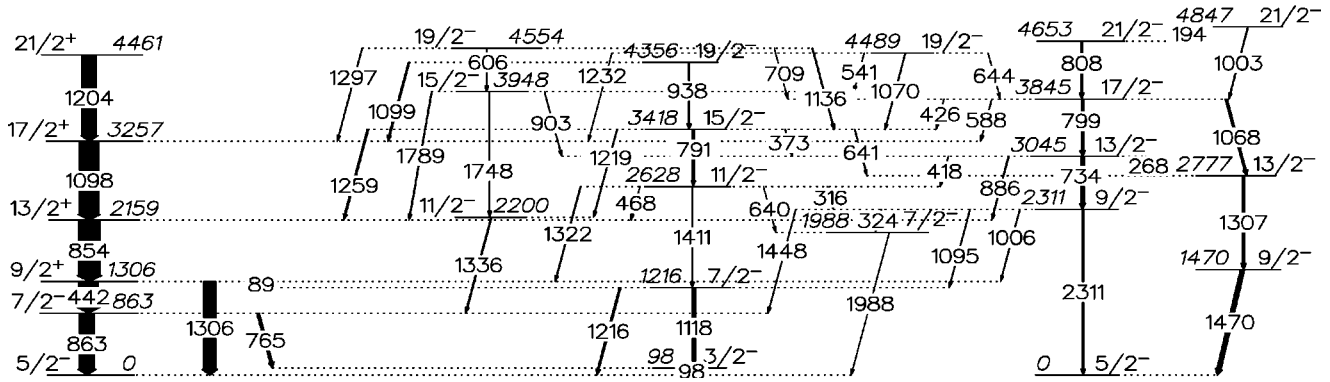

FIG. 2. Low-lying negative-parity states in ^{69}As obtained from the present work. The widths of the arrows are proportional to the γ-ray intensities.

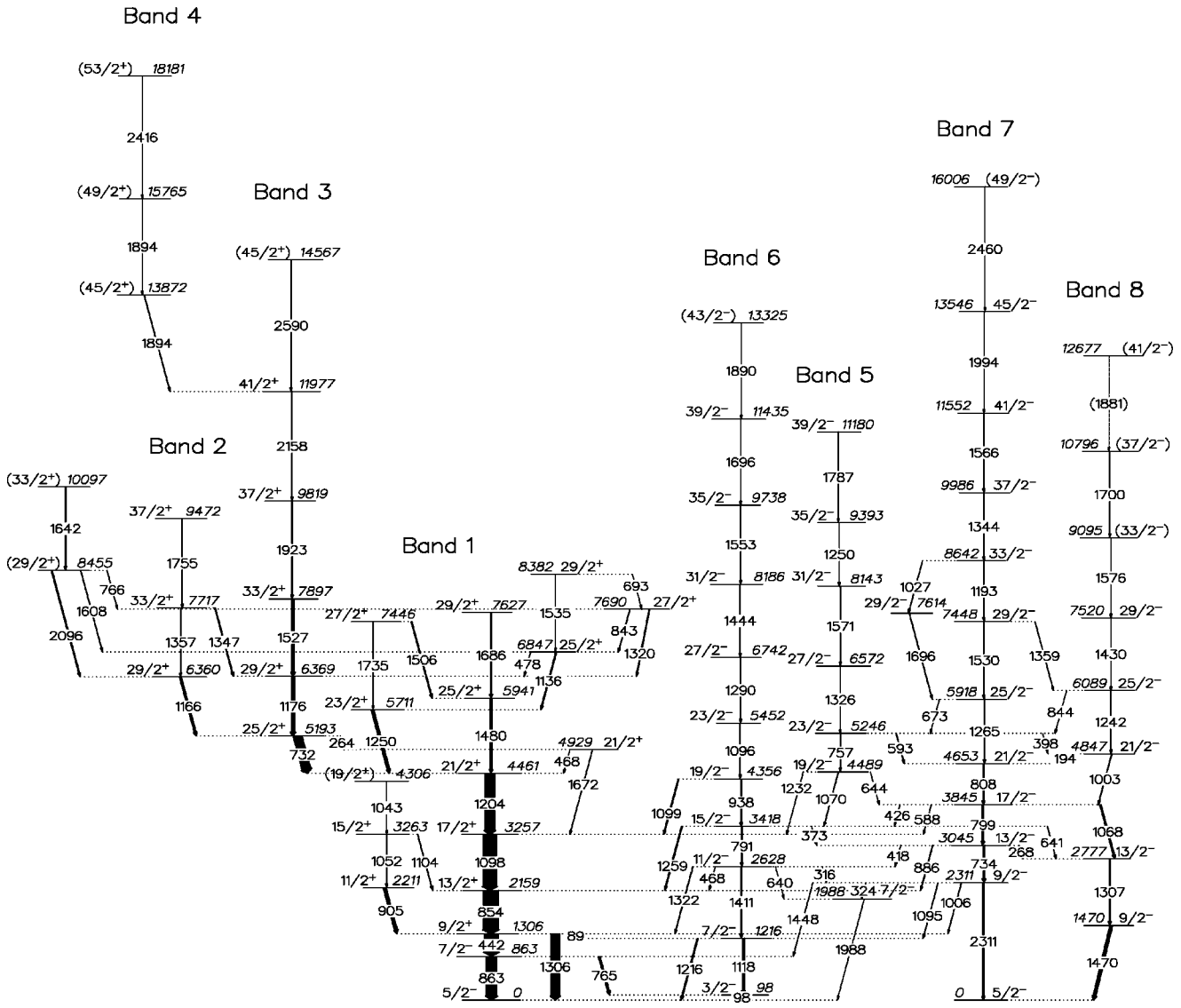

FIG. 3. High-spin states in ^{69}As obtained from the present analysis.

to an excitation energy of 5.2 MeV have been investigated in detail in the work of Hellmeister *et al.* [7]. Within that work, on the basis of γ-γ coincidences, angular distributions, and excitation functions, a rotational aligned $g_{9/2}$ proton band has been established. Their proposed level scheme consists mainly of the favored yrast structure observed up to spin $25/2^+$. In the unfavored yrast band only the $11/2^+$ and $15/2^+$ states could be identified [7]. The proposed protonic character for the $g_{9/2}$ band was later confirmed by the measurement of the magnetic moment $[\mu=(4.64\pm0.59)\mu_N]$ of the $I^\pi=9/2^+$, 1305.6-keV level [24]. The recent works of Mitarai *et al.* [10] and Bruce *et al.* [11] confirmed the existence of the levels found by Hellmeister and co-workers [7] and extended the favored yrast structure up to spins $33/2^+$ and $(41/2^+)$, respectively.

The low-lying level scheme of ^{69}As deduced from our coincidence measurements is shown in Figs. 1 (positive-parity states) and 2 (negative-parity states). The high-spin states obtained from the present analysis are presented in Fig. 3. The level structure contains many newly introduced levels as compared to the previous work [10,11]. Examples of doubly gated co-incidence spectra, revealing the newly observed transitions in ^{69}As, are shown in Fig. 4. The respective spectra were extracted mainly from the $\gamma\gamma\gamma$ cube because of the better statistics compared to the $3p$-$\gamma\gamma\gamma$ cube. The low-lying non-yrast states were better populated in the experiment at 95 MeV, while in the analysis of the high-spin states the 105 MeV data set has been used.

The results of the level determinations, γ energies, intensities, DCO ratios, multipolarities, and spin assignments are given in Table I.

A. Positive-parity states

1. Low-lying non-yrast states

Prior to this work, no non-yrast states of positive parity were known in ^{69}As. The double-gating procedure using known transitions depopulating the unfavored yrast structure led to the identification of new states at 2808.0, 3507.1, 3660.4, 3840.2, and 4148.2 keV (see Fig. 1). Good statistics

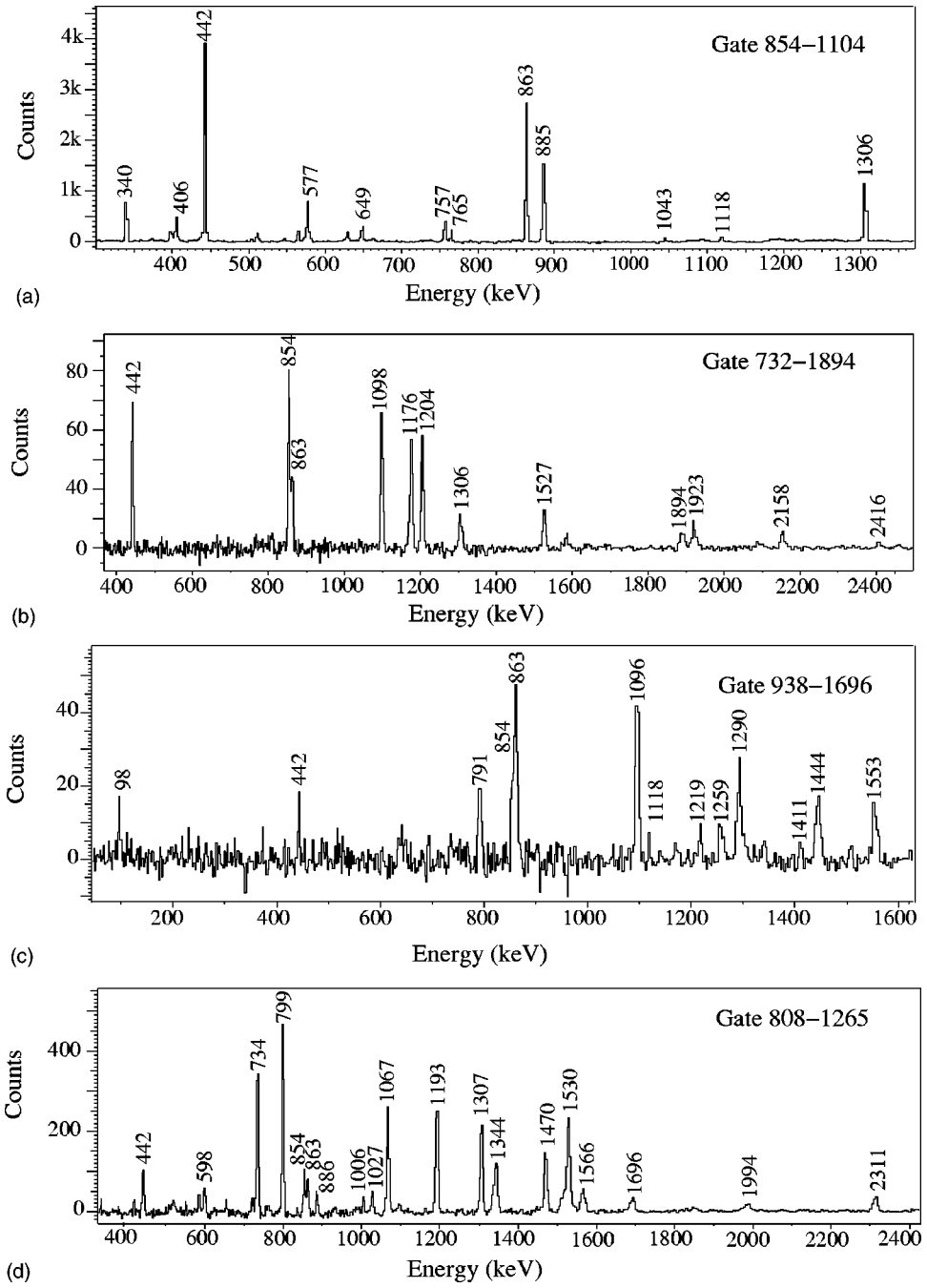

FIG. 4. Examples of doubly gated coincidence spectra from the $\gamma\gamma\gamma$ cube. (a) presents a spectrum acquired from the experiment at 95 MeV using the gold-backed ^{40}Ca target and (b), (c), and (d) contain spectra acquired from the experiment at 105 MeV using the self-supporting target. Peaks labeled with their energies in keV are assigned to ^{69}As.

made it possible to extract the multipole order of the transitions depopulating these levels supporting the spin assignments of $13/2^+, 15/2^+, 17/2^+, 17/2^+$ and $17/2^+$, respectively. The spectrum presented in Fig. 4(a) shows a double gate on the 853.8-1103.8 keV transitions. All the $17/2^+$ states enumerated above have a decay branch to the $15/2^+$ state at 3263.2 keV via the 397.2-, 577.0-, and 885.0-keV γ rays. The investigation of the doubly gated spectra using gates on intense transitions depopulating the favored yrast band revealed a second decay path of the newly observed levels to the yrast levels, thus confirming their placement in the level scheme of ^{69}As.

The new state at 2169.0 keV was found to decay via the 635.0-, 952.7-, and 1305.8-keV transitions. The DCO ratio obtained by gating on the intense 863.2-keV γ ray ($\Delta I=1$) is consistent with a $\Delta I=1$ character for the 1305.8-keV line, suggesting an $I=9/2$ spin assignment for the level at 2169.0 keV (see Fig. 1 and Table I). This level is populated by the 639.0-keV transition decaying from the positive-parity state at 2808.0 keV. No feeding from higher negative-parity levels

TABLE I. Energies, relative intensities, and DCO ratios of γ-ray transitions assigned to ^{69}As. The intensities are normalized to the 853.8-keV transition, set to be 100.

E_{level} (keV)	E_γ (keV)	I_γ[a]	R_{DCO}	Gate	σL	I_i^π	I_f^π
0.0						$5/2^-$	
98.2	98.2(3)	7.8(3)	0.50(5)[b]	1097.6	$M1/E2$	$3/2^-$	$5/2^-$
863.2	765.0(4)	11.9(29)	1.85(15)[b]	442.4	$E2$	$7/2^-$	$3/2^-$
	863.2(5)	69.1(29)	0.61(5)[b]	1097.6	$M1/E2$	$7/2^-$	$5/2^-$
1216.3	1118.1(3)	15.8(10)	1.36(12)[c]	799.2	$E2$	$7/2^-$	$3/2^-$
	1216.3(5)	6.9(14)	0.41(6)[c]	799.2	$M1/E2$	$7/2^-$	$5/2^-$
1305.6	89.3(2)	3.5(10)	0.46(6)[b]	1097.6	$E1$	$9/2^+$	$7/2^-$
	442.4(5)	91.7(44)	0.65(5)[b]	1204.2	$E1$	$9/2^+$	$7/2^-$
	1305.6(4)	58.4(62)	1.05(7)[b]	1097.6	$M2$	$9/2^+$	$5/2^-$
1470.3	1470.3(2)	18.9(16)	0.98(7)[b]	808.3	$E2$	$9/2^-$	$5/2^-$
1534.0	228.4(3)	0.22(3)			$(E2)$	$(5/2^+)$	$9/2^+$
	1435.8(4)	3.1(3)			$(E1)$	$(5/2^+)$	$3/2^-$
1987.5	1987.5(2)	0.19(1)	0.42(1)[c]	790.9	$M1/E2$	$7/2^-$	$5/2^-$
2159.4	853.8(5)	100	1.01(6)[b]	1097.6	$E2$	$13/2^+$	$9/2^+$
2169.0	635.0(3)	0.33(6)	2.2(7)[b]	648.5	$(E2)$	$9/2^{(+)}$	$(5/2^+)$
	952.7(2)	0.20(3)			$(E1)$	$9/2^{(+)}$	$7/2^-$
	1305.8(3)	2.1(3)	2.5(3)[c]	863.2	$(E1)$	$9/2^{(+)}$	$7/2^-$
2199.7	1336.5(2)	4.1(2)	2.3(2)[c]	863.2	$E2$	$11/2^-$	$7/2^-$
2210.7	905.1(3)	19.5(10)	0.19(4)[c]	756.9	$M1/E2$	$11/2^+$	$9/2^+$
2311.2	323.7(3)	0.18(4)	0.64(13)[c]	808.3	$M1/E2$	$9/2^-$	$7/2^-$
	1005.6(5)	1.5(1)	0.61(6)[c]	808.3	$E1$	$9/2^-$	$9/2^+$
	1094.9(4)	1.18(9)			$M1/E2$	$9/2^-$	$7/2^-$
	1448.0(4)	0.8(5)			$M1/E2$	$9/2^-$	$7/2^-$
	2311.2(3)	6.4(7)	1.08(9)[b]	808.3	$E2$	$9/2^-$	$5/2^-$
2627.6	316.4(2)	0.18(3)	0.57(13)[c]	790.9	$M1/E2$	$11/2^-$	$9/2^-$
	468.2(3)	<0.1	0.7(3)[b]	790.9	$E1$	$11/2^-$	$13/2^+$
	640.1(2)	0.2(4)	1.3(2)[c]	790.9	$E2$	$11/2^-$	$7/2^-$
	1322.0(5)	2.4(1)	0.67(6)[c]	790.9	$E1$	$11/2^-$	$9/2^+$
	1411.3(1)	5.0(3)	0.95(18)[c]	756.9	$E2$	$11/2^-$	$7/2^-$
2777.1	1306.8(3)	11.4(12)	1.01(8)[b]	1470.3	$E2$	$13/2^-$	$9/2^-$
2808.0	597.3(4)	3.6(7)	0.34(5)[c]	756.9	$M1/E2$	$13/2^+$	$11/2^+$
	639.0(4)	1.2(1)	1.7(2)[b]	648.5	$E2$	$13/2^+$	$9/2^{(+)}$
	648.6(2)	2.1(2)			$M1$	$13/2^+$	$13/2^+$
	1502.4(4)	4.7(10)	2.1(3)[b]	648.5	$E2$	$13/2^+$	$9/2^+$
3045.4	268.3(2)	0.12(1)	0.68(9)[c]	1470.3	$M1$	$13/2^-$	$13/2^-$
	334.4(1)	5.3(4)	0.51(5)[c]	799.2	$M1/E2$	$13/2^-$	$11/2^-$
	379.4(3)	1.6(1)			$M1/E2$	$13/2^-$	$11/2^-$
	417.8(4)	0.41(3)	0.52(7)[c]	808.3	$M1/E2$	$13/2^-$	$11/2^-$
	601.3(2)	0.91(6)	0.96(17)[c]	808.3	$E2$	$13/2^-$	$9/2^-$
	734.2(4)	14.3(17)	1.15(11)[b]	808.3	$E2$	$13/2^-$	$9/2^-$
	886.0(2)	3.2(2)	1.1(1)[c]	808.3	$E1$	$13/2^-$	$13/2^+$
3257.0	449.0(4)	<0.1			$E2$	$17/2^+$	$13/2^+$
	1097.6(2)	90.2(44)	0.95(6)[b]	1204.2	$E2$	$17/2^+$	$13/2^+$
3263.2	455.2(5)	0.11(3)			$M1/E2$	$15/2^+$	$13/2^+$
	1052.5(4)	1.55(4)	1.08(21)[c]	756.9	$E2$	$15/2^+$	$11/2^+$
	1103.8(2)	1.9(5)	0.19(2)[c]	756.9	$M1/E2$	$15/2^+$	$13/2^+$
3418.5	373.1(4)	1.0(2)			$M1/E2$	$15/2^-$	$13/2^-$
	641.4(3)	1.7(4)	0.67(10)[c]	1470.3	$M1/E2$	$15/2^-$	$13/2^-$

TABLE I. (*Continued.*)

E_{level} (keV)	E_γ (keV)	I_γ[a]	R_{DCO}	Gate	σL	I_i^π	I_f^π
	790.9(2)	7.6(14)	1.2(1)[b]	756.9	$E2$	$15/2^-$	$11/2^-$
	1218.8(3)	2.1(4)	0.77(10)[c]	756.9	$E2$	$15/2^-$	$11/2^-$
	1259.1(2)	6.1(3)	0.49(6)[b]	756.9	$E1/M2$	$15/2^-$	$13/2^+$
3507.1	699.1(3)	<0.1			$M1/E2$	$15/2^+$	$13/2^+$
	1296.4(4)	0.32(4)	1.12(6)[b]	1305.6	$E2$	$15/2^+$	$11/2^+$
	1347.7(3)	0.24(3)	0.41(16)[c]	756.9	$M1/E2$	$15/2^+$	$13/2^+$
3660.4	153.3(5)	0.16(1)			$M1/E2$	$17/2^+$	$15/2^+$
	397.2(3)	0.17(1)	0.57(13)[c]	1052.5	$M1/E2$	$17/2^+$	$15/2^+$
	403.4(2)	2.7(2)			$M1$	$17/2^+$	$17/2^+$
	852.4(3)	4.4(3)	1.24(5)[b]	853.8	$E2$	$17/2^+$	$13/2^+$
	1501.0(3)	4.1(3)	1.76(14)[c]	853.8	$E2$	$17/2^+$	$13/2^+$
3840.2	333.1(3)	1.9(6)	0.49(23)[c]	756.9	$M1/E2$	$17/2^+$	$15/2^+$
	577.0(4)	3.5(12)	0.39(6)[c]	756.9	$M1/E2$	$17/5^+$	$15/2^+$
	583.2(4)	<0.1			$M1$	$17/2^+$	$17/2^+$
	1032.2(2)	5.7(4)	1.3(1)[b]	853.8	$E2$	$17/2^+$	$13/2^+$
	1680.8(6)	1.9(6)	1.15(27)[c]	756.9	$E2$	$17/2^+$	$13/2^+$
3844.6	426.1(3)	0.17(1)	0.76(13)[c]	790.9	$M1/E2$	$17/2^-$	$15/2^-$
	587.6(3)	0.86(6)	1.25(20)[c]	808.3	$E1$	$17/2^-$	$17/2^+$
	799.2(3)	12.1(12)	1.01(8)[b]	808.3	$E2$	$17/2^-$	$13/2^-$
	1067.5(2)	8.9(8)	1.01(8)[b]	808.3	$E2$	$17/2^-$	$13/2^-$
3947.5	902.3(3)	1.00(5)			$M1/E2$	$15/2^-$	$13/2^-$
	1748.0(4)	3.1(4)	2.91(55)[c]	863.2	$E2$	$15/2^-$	$11/2^-$
	1788.7(4)	2.6(3)	0.44(9)[c]	853.8	$E1$	$15/2^-$	$13/2^+$
4148.2	641.1(2)	0.25(2)	0.80(14)[c]	756.9	$M1/E2$	$17/2^+$	$15/2^+$
	885.0(4)	0.14(2)	0.56(8)[c]	756.9	$M1/E2$	$17/2^+$	$15/2^+$
	891.2(2)	<0.1			$M1$	$17/2^+$	$17/2^+$
4306.1	465.9(4)	<0.1			$(M1/E2)$	$(19/2^+)$	$17/2^+$
	645.7(3)	0.12(3)			$(M1/E2)$	$(19/2^+)$	$17/2^+$
	1042.9(3)	0.24(5)			$(E2)$	$(19/2^+)$	$15/2^+$
4356.2	937.7(2)	5.4(3)	1.23(12)[b]	853.8	$E2$	$19/2^-$	$15/2^-$
	1099.2(5)	5.6(6)			$E1$	$19/2^-$	$17/2^+$
4461.2	1204.2(1)	68.2(31)	1.16(7)[b]	1097.6	$E2$	$21/2^+$	$17/2^+$
4488.7	340.5(3)	0.8(1)	0.42(3)[c]	756.9	$E1$	$19/2^-$	$17/2^+$
	541.0(3)	0.22(3)	1.23(25)[c]	756.9	$E2$	$19/2^-$	$15/2^-$
	644.1(4)	<0.1			$M1/E2$	$19/2^-$	$17/2^-$
	648.5(2)	1.4(2)	0.55(6)[c]	756.9	$E1$	$19/2^-$	$17/2^+$
	828.3(4)	0.8(1)	0.53(7)[c]	756.9	$E1$	$19/2^-$	$17/2^+$
	1070.2(3)	1.6(1)	1.04(8)[b]	756.9	$E2$	$19/2^-$	$15/2^-$
	1231.7(5)	0.12(2)	0.53(11)[b]	756.9	$E1$	$19/2^-$	$17/2^+$
4554.0	405.8(3)	2.1(5)			$E1$	$19/2^-$	$17/2^+$
	606.3(3)	2.5(8)			$E2$	$19/2^-$	$15/2^-$
	709.4(1)	0.17(4)	0.33(7)[c]	799.2	$M1/E2$	$19/2^-$	$17/2^-$
	893.6(3)	2.4(4)	0.39(10)[c]	1097.6	$E1$	$19/2^-$	$17/2^+$
	1135.5(2)	2.9(12)	1.4(3)[c]	790.9	$E2$	$19/2^-$	$15/2^-$
	1297.0(4)	1.4(4)	0.54(4)[b]	1097.6	$E1$	$19/2^-$	$17/2^+$
4652.9	808.3(2)	6.3(4)	0.93(8)[b]	1470.3	$E2$	$21/2^-$	$17/2^-$
4713.3	565.1(5)	<0.1					$17/2^+$
4847.2	194.3(3)	0.11(2)	0.54(7)[c]	808.3	$M1$	$21/2^-$	$21/2^-$

TABLE I. (*Continued.*)

E_{level} (keV)	E_γ (keV)	I_γ[a]	R_{DCO}	Gate	σL	I_i^π	I_f^π
	1002.6(5)	2.3(2)	0.94(7)[b]	1470.3	$E2$	$21/2^-$	$17/2^-$
4929.4	468.2(1)	0.27(2)			$M1$	$21/2^+$	$21/2^+$
	1672.4(6)	1.2(1)	1.39(14)[b]	1097.6	$E2$	$21/2^+$	$17/2^+$
5150.0	436.7(3)	<0.1					
5152.3	598.3(2)	3.1(7)					$19/2^-$
5193.3	263.8(2)	0.5(1)			$E2$	$25/2^+$	$21/2^+$
	732.1(4)	57.6(27)	0.94(6)[b]	1097.6	$E2$	$25/2^+$	$21/2^+$
5245.6	398.4(3)	1.13(8)	0.51(8)[c]	808.3	$M1/E2$	$23/2^-$	$21/2^-$
	592.7(2)	2.8(2)	0.36(3)[c]	808.3	$M1/E2$	$23/2^-$	$21/2^-$
	691.6(4)	1.25(9)	0.9(2)[b]	799.2	$E2$	$23/2^-$	$19/2^-$
	756.9(2)	1.35(1)	0.94(13)[b]	790.9	$E2$	$23/2^-$	$19/2^-$
5452.4	1096.2(5)	3.4(2)	0.94(7)[b]	937.7	$E2$	$19/2^-$	$15/2^-$
5711.1	1249.9(3)	17.4(8)	0.47(5)[b]	1097.6	$M1/E2$	$23/2^+$	$21/2^+$
5918.3	672.7(5)	0.29(2)	0.51(9)[c]	756.9	$M1/E2$	$25/2^-$	$23/2^-$
	1265.4(3)	4.0(3)	1.00(8)[b]	799.2	$E2$	$25/2^-$	$21/2^-$
5941.0	1479.8(1)	12.3(5)	0.84(6)[b]	1204.2	$E2$	$25/2^+$	$21/2^+$
6089.2	843.6(3)	0.43(3)			$M1/E2$	$25/2^-$	$23/2^-$
	1242.0(4)	1.6(1)	1.22(14)[b]	799.2	$E2$	$25/2^-$	$21/2^-$
6359.7	1166.4(5)	12.5(6)	1.03(19)[b]	1097.6	$E2$	$29/2^+$	$25/2^+$
6369.4	1176.1(2)	25.4(11)	1.04(12)[b]	1097.6	$E2$	$29/2^+$	$25/2^+$
6571.5	1325.9(4)	1.1(1)	1.07(8)[b]	756.9	$E2$	$27/2^-$	$23/2^-$
6742.0	1289.6(3)	2.5(2)	1.28(13)[b]	937.7	$E2$	$27/2^-$	$23/2^-$
6847.3	477.9(3)	0.62(17)	1.28(13)[b]	1176.1	$E2$	$25/2^+$	$29/2^+$
	1136.2(5)	6.0(17)	0.47(7)[b]	1097.6	$M1/E2$	$25/2^+$	$23/2^+$
7446.5	1505.5(6)	5.6(7)	0.35(3)[b]	1204.4	$E2$	$27/2^+$	$25/2^+$
	1735.4(5)	0.23(3)			$E2$	$27/2^+$	$23/2^+$
7448.3	1359.1(3)	1.08(8)			$E2$	$29/2^-$	$25/2^-$
	1530.0(4)	2.8(2)	1.49(11)[b]	1265.4	$E2$	$29/2^-$	$25/2^-$
7519.5	1430.3(5)	0.73(6)	0.93(10)[b]	799.2	$E2$	$29/2^-$	$25/2^-$
7614.5	1696.2(3)	1.8(6)	1.43(10)[b]	808.3	$E2$	$29/2^-$	$25/2^-$
7627.2	1686.2(3)	1.2(2)	1.2(3)[b]	1204.2	$E2$	$29/2^+$	$25/2^+$
7689.9	842.6(2)	1.8(4)	0.45(13)[b]	1136.2	$M1/E2$	$27/2^+$	$25/2^+$
	1320.5(2)	4.9(13)	0.36(5)[b]	1176.1	$M1/E2$	$27/2^+$	$29/2^+$
7716.7	1347.4(3)	4.9(3)	1.2(2)[b]	1176.1	$E2$	$33/2^+$	$29/2^+$
	1357.1(2)	4.1(2)	1.32(10)[b]	1166.4	$E2$	$33/2^+$	$29/2^+$
7896.6	1527.2(4)	18.9(8)	1.15(8)[b]	1176.1	$E2$	$33/2^+$	$29/2^+$
8142.8	1571.3(5)	0.64(5)	0.98(10)[b]	756.9	$E2$	$31/2^-$	$27/2^-$
8185.8	1443.8(6)	1.3(2)	1.06(8)[b]	937.7	$E2$	$31/2^-$	$27/2^-$
8382.4	692.5(2)	0.12(2)	0.50(11)[b]	1320.5	$M1/E2$	$29/2^+$	$27/2^+$
	1535.1(5)	0.3(1)	1.16(13)[b]	1136.2	$E2$	$29/2^+$	$25/2^+$
8455.4	765.5(3)	0.9(2)			$(M1/E2)$	$(29/2^+)$	$27/2^+$
	1608.1(3)	1.98(55)			$(E2)$	$(29/2^+)$	$25/2^+$
	2095.7(7)	6.1(17)	1.27(11)[b]	1204.2	$(M1)$	$(29/2^+)$	$29/2^+$
8641.5	1193.2(4)	2.9(2)	1.05(9)[b]	799.2	$E2$	$33/2^-$	$29/2^-$
	1027.0(3)	1.1(3)			$E2$	$33/2^-$	$29/2^-$
9095.4	1575.9(4)	0.6(1)			$(E2)$	$(33/2^-)$	$29/2^-$
9393.0	1250.2(5)	0.18(2)	1.25(17)[b]	756.9	$E2$	$35/2^-$	$31/2^-$
9472.2	1755.4(7)	3.1(2)	0.97(20)[b]	1166.4	$E2$	$37/2^+$	$33/2^+$

TABLE I. (*Continued.*)

E_{level} (keV)	E_γ (keV)	I_γ[a]	R_{DCO}	Gate	σL	I_i^π	I_f^π
9738.5	1552.7(3)	0.8(1)	0.90(8)[b]	937.7	$E2$	$35/2^-$	$31/2^-$
9819.4	1922.8(6)	6.2(3)	1.4(1)[b]	1204.2	$E2$	$37/2^+$	$33/2^+$
9985.7	1344.2(5)	2.3(2)	1.03(8)[b]	1265.4	$E2$	$37/2^-$	$33/2^-$
10097.0	1641.6(4)	3.9(3)			($E2$)	($29/2^+$)	($25/2^+$)
10795.8	1700.4(4)	0.80(5)			($E2$)	($37/2^-$)	($33/2^-$)
11180.3	1787.3(3)	0.16(2)	1.2(2)[b]	757.6	$E2$	$39/2^-$	$35/2^-$
11434.6	1696.1(6)	0.4(1)	1.5(2)[b]	937.7	$E2$	$39/2^-$	$35/2^-$
11551.8	1566.1(5)	2.3(2)	1.15(10)[b]	1265.4	$E2$	$41/2^-$	$37/2^-$
11977.2	2157.8(4)	2.9(1)	1.15(14)[b]	1176.1	$E2$	$41/2^+$	$37/2^+$
12677.0	1881.4(2)	0.4(1)			($E2$)	($41/2^-$)	($37/2^-$)
13325.0	1890.4(3)	0.2(1)			($E2$)	($43/2^-$)	$39/2^-$
13545.8	1994.0(2)	0.50(6)	0.96(10)[b]	1193.2	$E2$	$45/2^-$	$41/2^-$
13871.5	1894.3(4)	2.1(3)			($E2$)	($45/2^+$)	($41/2^+$)
14567.0	2589.8(3)	1.8(4)			($E2$)	($45/2^+$)	$41/2^+$
15765.0	1893.5(5)	1.6(4)			($E2$)	($49/2^+$)	($45/2^+$)
16005.6	2459.8(3)	0.3(2)			($E2$)	($49/2^-$)	$45/2^-$
18180.6	2415.6(2)	1.23(6)			($E2$)	($53/2^+$)	($49/2^+$)

[a]Relative intensities derived from the $3p$-$\gamma\gamma$ matrix sorted from the self-supporting target experiment.
[b]DCO ratio deduced from the $3p$-$\gamma\gamma$ matrix sorted from the self-supporting target experiment.
[c]DCO ratio determined from the $3p$-$\gamma\gamma$ matrix sorted from the backed-target experiment.

has been observed. Therefore, a positive parity is tentatively proposed for the 2169.0-keV level, although negative parity cannot be excluded. The coincidence data revealed the existence of a state at 1534.0 keV which decays mainly to the first negative-parity excited level of 98.2 keV. A $5/2^+$ state close in energy with the yrast $9/2^+$ state exists in the heavier ^{71,73,75,77}As isotopes, investigated by the (^{3}He,d) transfer reaction in the work of Betts *et al.* [3]. Within that work, based on measured deuteron angular distributions, spins and parities $5/2^+$ for the respective states have been assigned. Such assignment is also in agreement with the theoretical predictions [3]. Consequently, spin parity ($5/2^+$) is assigned to the state at 1534.0 keV in ^{69}As.

The DCO ratios of the 340.5-, 648.5-, and 828.3-keV transitions populating the three $17/2^+$ newly observed states indicate dipole character, which results in the assignment of $I=19/2$ for the level at 4488.7 keV. A positive-parity assignment for this level would imply the existence of at least one stretched $E2$ transition to one of the $15/2^+$ states but there is no experimental evidence for such transitions. Similar decay sequences have been also observed in the light ^{65,67,69}Ge isotopes [25–27]. Polarization measurements for the $19/2 \rightarrow 17/2^+$ connecting transitions were always consistent with an electric character, leading to a negative-parity assignment for the states of spin $I=19/2$ [25–27]. Such decays have already been observed in ^{71}As, where three $19/2^{(-)}$ levels have been found, each of them populating at least one of the $17/2^+$ levels [12]. Therefore, a negative-parity assignment for the state at 4488.7 keV is proposed.

The coincidence data for ^{69}As show clear evidence for the existence of two other $I^\pi=19/2$ states at 4554.0 and 4356.2 keV, respectively. The observation of several decaying transitions to the negative-parity states and the systematic features discussed above in connection with the $I=19/2$ state at 4488.7 keV suggest negative-parity assignments to both levels.

2. Positive-parity rotational structures

Band 1. This band includes the previously known yrast levels below spin $21/2^+$ and the new levels at 4306.1, 5711.1, 5941.0, 7446.5, and 7627.2 keV (Fig. 3). The low intensities of the 465.9-, 645.7-, and 1042.9-keV transitions depopulating the state at 4306.1 keV prevent DCO measurements and firm spin assignment for the newly observed level. Likely spin values for this state would be $17/2$ and $19/2$ and positive parity since only decay branches toward the positive-parity states have been observed. A spin parity $17/2^+$ would further imply the existence of at least one populating transition from the newly identified $19/2^-$ states, in agreement with the systematics. Since no such transition could be observed, a tentative spin of $19/2^+$ is assigned to the level at 4306.1 keV. The DCO ratios of the 1479.8- and 1686.2-keV γ rays are both consistent with a stretched $E2$ character, supporting the $25/2^+$ and $29/2^+$ spin assignments for the levels at 5941.0 and 7627.2 keV, respectively (see Table I). The state of spin $23/2^+$ at 5711.1 keV found in Ref. [10] has been confirmed in the present work. In fact, the sequence consisting of levels at 5711.1, 5941.0, 7446.5, and 7627.2 keV exhibits the same degree of signature splitting as the yrast sequence below spin $21/2^+$. This makes the newly observed sequence a candidate for the continuation of the ground-state band at higher spins.

Band 2. Above spin $I^\pi=25/2^+$ a forking into two almost degenerate $I^\pi=29/2^+$ states occurs. The level at 6359.7 keV

is yrast and is fed by a cascade consisting of 1357.1- and 1755.4-keV transitions depopulating the states at 7716.8 and 9472.2 keV, respectively (Fig. 3). The spin $I^{\pi}=29/2^{+}$ of the 6359.7-keV yrast state is fixed by the DCO ratio of the 1166.4-keV γ ray, whereas the spin $I^{\pi}=33/2^{+}$ of the 7716.8-keV yrast level is fixed by the DCO ratio of the 1347.4-keV γ ray populating the second $29/2^{+}$ state, at 6369.4 keV. Although band 2 is yrast in the $29/2^{+}$–$(37/2^{+})$ spin region, it carries little flux and the higher-spin configurations decay mainly to the second $29/2^{+}$ state (band 3 in Fig. 3).

Band 3. The results of the current investigations have confirmed the states up to spin $37/2^{+}$ reported in the work of Bruce *et al.* [11]. A γ ray of 2091 keV has been previously observed [11] as feeding the $37/2^{+}$ level of this band. The data from the present experiments do not show any coincidence relation which would support the placement of a 2091-keV transition on top of the level at 9819.4 keV. Instead, this level was found to be populated by the 2157.8-keV γ ray whose DCO ratio is consistent with a stretched $E2$ character. Band 3 has been extended up to a tentative spin of $(45/2^{+})$.

Band 4. Around spin $41/2^{+}$ band 3 is found from the present analysis to be crossed by the structure labeled as band 4 in the level scheme of Fig. 3. The poor statistics and the presence of the 1894-keV doublet prevent DCO measurements in this high-spin region; therefore the spins of the observed states are only tentatively assigned. Figure 4(b) shows a 732.1-1894.3 keV doubly gated spectrum. The chosen double gate selects only the transitions in bands 3 and 4, and constitutes a firm evidence for the placement of the second 1893.5-keV transition in the level scheme of ^{69}As.

Other positive-parity bands. The coincidence analysis supports the placement in the level scheme of ^{69}As of two other positive-parity structures. The states at 6847.3, 7689.9, and 8382.4 keV form a spin sequence $25/2^{+}$-$27/2^{+}$-$29/2^{+}$. The spin $27/2^{+}$ assigned to the level at 7689.9 keV is based on the DCO value of the 1320.5-keV transition which is consistent with a dipole character. A quadrupole 1322-keV transition has been reported in Ref. [10], which is most likely the 1320.5-keV transition discussed above. The present data support its placement but not the spin. The second new sequence consists of the 8455.4- and 10 097.0-keV states. The DCO ratio of the 2095.7-keV transition is consistent with a quadrupole character suggesting an $I^{\pi}=33/2^{+}$ spin assignment for the level at 8455.4 keV. The observation of the 765.5- and 1608.1-keV transitions populating the firmly established $27/2^{+}$ state at 7689.9 keV and the $25/2^{+}$ state at 6847.3 keV, respectively, rules out the $I^{\pi}=33/2^{+}$ spin value for the state at 8455.4 keV. Therefore, a spin $I^{\pi}=29/2^{+}$ has been proposed for this state.

B. Negative-parity states

1. Low-lying negative-parity states

The first negative-parity excited state lies at only 98.2 keV excitation energy (see Fig. 2). From angular distribution measurements, a spin $I^{\pi}=3/2^{-}$ has been assigned to this level [28]. The two $9/2^{-}$ levels at 1470.3 and 2311.2 keV have been reported by Mitarai *et al.* in Ref. [10]. The state at 1470.3 keV was found to be fed by an $E2$ transition of 1306.8 keV decaying from the state at 2777.1 keV. Furthermore, the sequence consisting of the 1470.3-, 1306.8-, and 1067.5-keV quadrupole transitions was found to form a decay path parallel to the 2311.2-, 734.2-, and 799.2-keV transitions with the level at 3844.6 keV as a common level [10]. Bruce and coworkers confirmed the decay pattern observed by Mitarai *et al.* [10] and assigned spins and parities to the involved states [11].

The two sequences have been well populated in both data sets used in the present analysis and the DCO ratios for the connecting transitions could be extracted with good accuracy. The ratios are all consistent with a quadrupole character supporting the $13/2^{-}$ spin assignment for the states at 2777.1 and 3045.4 keV, $17/2^{-}$ for the state at 3844.7 keV, and $21/2^{-}$ for the state at 4652.9 keV (see Fig. 2 and Table I). A third new, rather well populated sequence consisting of the levels at 1216.3, 2627.6, and 3418.5 keV has been observed on top of the 98.2-keV level. The DCO ratios of the 1118.1-, 1411.3-, and 790.9-keV γ rays are compatible with a $\Delta I=2$ character, supporting the $7/2^{-}$, $11/2^{-}$, and $15/2^{-}$ spin assignment for the respective levels. The negative-parity assignment to the levels at 2627.6 and 3418.5 keV is also supported by the observation of the weak cascade of dipole γ rays between these levels and the firmly established negative-parity levels at 2311.1 and 3045.4 keV. The excitation energy of 3418.5 keV and the existence of the decay branch to the yrast $13/2^{+}$ state makes the $I^{\pi}=15/2^{-}$ state a candidate for the octupole state in ^{69}As, in agreement with the systematics [26,27]. The second candidate for the octupole state in ^{69}As is the newly observed level at 3947.5 keV.

2. Negative-parity rotational structures

Band 5. This band was identified for the first time in the present analysis. The spin assignments were deduced from the measured DCO ratios which are close to 1.0 for all inband transitions, hence giving evidence for the $\Delta I=2$ nature of these γ rays. The band is yrast and shows an irregularity around spin $31/2^{-}$ (Fig. 3). The maximum spin observed in band 5 is $39/2^{-}$, which corresponds to an excitation energy of 11 180.3 keV.

Band 6. This band is also new and is better populated than band 5. The DCO ratios of the inband transitions are all consistent with a stretched quadrupole character. Band 6 has been observed up to an excitation energy of 13 325.0 keV and a tentative spin of $(43/2^{-})$. The coincidence spectrum obtained by gating on the 937.7- and 1696.1-keV transitions is shown in Fig. 4(c). The transitions assigned to band 6 in ^{69}As are marked in the figure. No interband transitions connecting this band with the other negative-parity structures could be identified.

Band 7. On top of the level at 3844.6 keV two parallel bands develop (bands 7 and 8 in Fig. 3). Band 7 is yrast and is well populated in the experiment at 105-MeV beam energy. The levels at 4652.9 and 5918.3 keV which have been previously reported [10] are confirmed by the present analysis. The duplication of the $I^{\pi}=29/2^{-}$ levels around 7.5-MeV excitation energy may be connected with the irregularity in rotational energy observed in this spin region in band 7. The γ-ray spectrum in Fig. 4(d) shows several transitions, e.g.,

1530.0-, 1193.2-, and 1344.2-keV lines which were firmly assigned to band 7. The band has been extended up to an excitation energy of 16 005.6 keV and a tentative spin of $(49/2^-)$.

Band 8. This band was identified for the first time in the present analysis. Based on DCO measurements, the spins could be firmly assigned only to the low members of the band. However, band 8 does not show any irregularity in the spin region it is observed, appearing consistent with a rotational cascade of $E2$ transitions. Band 8 was populated in the present experiments up to a tentative spin of $(41/2^-)$ and 12 677.0 keV excitation energy (see Fig. 3).

IV. DISCUSSION

A. Low-lying positive-parity states

The low-lying positive-parity states in ^{69}As fit very well in the systematics of the light odd-mass As isotopes. General trends like the small splitting between the lowest $11/2^+$ and $13/2^+$ states and between the $15/2^+$ and $17/2^+$ states or the presence of the $9/2^+$-$5/2^+$ doublet at low excitation energies have already been discussed in the past [5–7].

The decoupled character of the yrast positive-parity bands suggests prolate deformations in the odd-mass As nuclei. Lifetime measurements in ^{69}As, employing the Doppler recoil-distance method led to a quadrupole deformation of $\beta_2 \approx 0.2$ for the yrast $13/2^+$ state and the deformation was found to decrease with increasing spin [7]. For the low members of the $g_{9/2}$ bands in the ^{71,73}As isotopes, larger and rather stable deformations $\beta_2 \approx 0.3$ have been extracted in the work of Heits *et al.* [5].

Several models have been proposed to describe the properties of the low-lying states in the odd-mass As nuclei. The investigations within the particle-core [5,7,29] formalism indicated that a deformed picture with the inclusion of the Coriolis coupling provides the most adequate first-order representation of odd-As isotopes. A better parametrization for the core taking into account the γ deformation and a variable moment of inertia (VMI) has been proposed by Toki and Faessler [30]. Within that approach, the small energy splittings between the $13/2^+$ and $11/2^+$ states and between the $17/2^+$ and $15/2^+$ states in ^{71,73}As are closely related to the triaxiality of the core [31]. Recently, an Interacting Boson Fermion Model (IBFM) treatment has been applied to the states below 1.5-MeV excitation energy in ^{73}As [32].

In the present work we succeeded to extend the ground-state band in ^{69}As above the crossing point and we found that with increasing spin, the splitting between the favored and the unfavored states slightly increases. Moreover, the intensities of the $E2$ transitions depopulating the favored band were found to decrease drastically above spin $21/2^+$. The kinematic ($J^{(1)}$) and the dynamic ($J^{(2)}$) moments of inertia for the favored band are plotted in Fig. 5. For comparison, the kinematic moments of inertia for the ground-state bands in ^{71}As [12] and ^{68}Ge [36] are also represented. Although the kinematic moment of inertia for the favored band in ^{69}As shows no clear evidence for a crossing, the peak around 0.53 MeV in the dynamic moment of inertia (Fig. 5, bottom) may

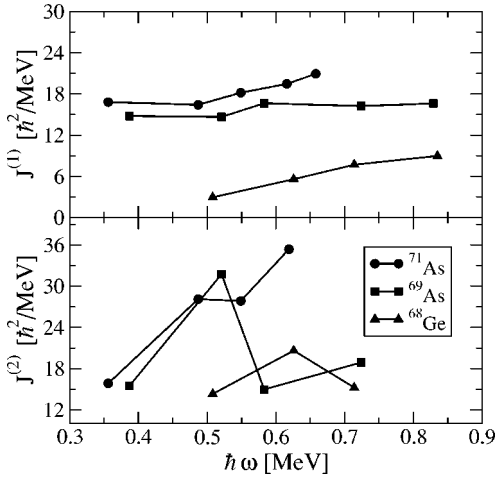

FIG. 5. Kinematic ($J^{(1)}$) and dynamic ($J^{(2)}$) moments of inertia for the band 1 in ^{69}As and ground-state bands in ^{71}As and ^{68}Ge. For the As nuclei, a value of $K=5/2$ has been used in the analysis.

reflect a band crossing within the sequence. We made an attempt to describe the states in band 1 by applying the rigid triaxial rotor plus particle model [33,34] with variable moment of inertia [30]. The triaxial rotor is called "rigid" because its shape is kept fixed throughout the calculation (the deformation parameters ε_2 and γ are constant). No single set of (ε_2, γ) could be found to reproduce the signature splitting and the level order in band 1 simultaneously. According to our calculations, the observed small splitting between the $11/2^+$ and $13/2^+$ states and between the $15/2^+$ and $17/2^+$ states can only be reproduced for γ values in the interval from 20° to 25°, whereas in order to fit the splitting between the higher-spin states we had to employ γ values greater than 30°. The calculations revealed an energy spectrum strongly dependent on the γ parameter, while the variation of the other model parameters (quadrupole deformation or the VMI parameters) does not have a strong influence on the fit. These results suggest a γ-soft low-lying spectrum in ^{69}As, which is in agreement with the expectations and the predictions of the calculated total Routhian surfaces (TRS's) for the As isotopes [11,12].

B. Low-lying negative-parity states

The negative-parity states in the nuclei of the $A \sim 70$ mass region are in general correlated with the single-particle excitation of the particles lying in the $p_{1/2}$, $p_{3/2}$, and $f_{5/2}$ shell-model orbitals. In ^{69}As, the states below 3-MeV excitation energy show a nonregular energy spacing, presumably being of single-particle character. Competing with these states, two main configurations could be distinguished. The configuration consisting of states at 1987.5, 2627.6, and 3418.5 keV may be considered the signature partner of the configuration consisting of states at 2311.2, 3045.4, and 3844.6 keV (see Fig. 2). This is justified by the occurrence of the weak $M1/E2$ crossover transitions between the levels of the two configurations.

Similar negative-parity structures have been identified previously in ^{71}As [12]. There, the $E2$ transitions in the band

built on the second $9/2^-$ state were found to show a high collectivity. Total Routhian calculations for the $\pi=-, \alpha=+1/2$ states in ^{71}As showed the presence of three shallow minima for rotational frequencies below 0.4 MeV [12]. The minima were located near $\gamma=0°$ and $\gamma=\pm 60°$. With increasing rotational frequency one triaxial minimum was calculated to persist. In a recent work, Fotiades *et al.* [13] extended the negative-parity band found in Ref. [12] up to spin $(37/2^-)$ and observed a new sequence of negative-parity levels developing at low excitation energies. The newly observed structure has been interpreted as being part of a strong-coupling-like band built on the $7/2^-[303]$ proton orbital which approaches the Fermi surface for $Z=33$ at large $\beta_2>0.3$ prolate deformations. The $f_{7/2}$ band in ^{71}As was found to be a $\Delta I=1$ sequence with $B(M1)/B(E2)$ ratios varying between 4 and 6 $\mu_N^2/(e^2\mathrm{b}^2)$ and could be reproduced with a quadrupole moment of $Q_t=3.1\ e$b which corresponds to the deformation $\beta_2=0.38$ [13].

A possible candidate for a $f_{7/2}$ band in ^{69}As could be the structure containing the levels discussed above. However, the properties of this structure do not really resemble those of the $f_{7/2}$ band found in ^{71}As. In ^{69}As, the $M1/E2$ crossover transitions between the favored and the unfavored members of the presumed $f_{7/2}$ band are very weak with respect to the intraband $E2$ transitions. The corresponding $B(M1)/B(E2)$ ratios calculated with the experimental branching ratios are found to vary between 0.04 and 2.1 $\mu_N^2/(e^2\mathrm{b}^2)$. Since the $M1$ strengths are proportional to the difference (g_K-g_R) and the gyromagnetic ratio for collective rotation is $g_R\approx 0.48$, such low values of the $B(M1)/B(E2)$ ratios indicate $g_K\approx g_R$ for this sequence. A near cancellation of (g_K-g_R) is expected to occur for a $5/2^-$ structure, but not for a $7/2^-$ band.

As pointed out in the previous section, the two $15/2^-$ states at 3418.5 and 3947.5 keV (see Fig. 2) are candidates for octupole states in ^{69}As. Such states are generated in the odd-A nuclei by coupling the $g_{9/2}$ particle to the 3^- state in the even-even core. Both states show the systematic features characteristic of the octupole states found in the neighboring odd-A nuclei, namely, the direct feeding via $E2$ transitions from the higher $19/2^-$ states and the decay via $E1$ transitions into the respective $13/2^+$ yrast level. In ^{68}Ge, the 3^- state has been observed at an excitation energy of 2649 keV [35]. By combining this energy with the excitation energy of the $g_{9/2}$ proton excitation in ^{69}As (1306 keV) we obtain an energy of 3955 keV, very close to the observed energy of 3947.5 keV of the second $15/2^-$ state in ^{69}As. Similarly, two of the three observed $19/2^-$ levels can be interpreted as coupling of the $g_{9/2}$ proton to the 5^- states at 3582 and 3649 keV in ^{68}Ge [35], even though the excitation energy of the $19/2^-$ states in ^{69}As is by some 300 keV lower than expected. Analogous discussions could be applied to the higher-spin states like $21/2^-(6^-)$ and $23/2^-(7^-)$.

C. High-spin positive-parity states

Figure 6 shows the kinematic $(J^{(1)})$ and the dynamic $(J^{(2)})$ moments of inertia for the three excited positive-parity bands 2, 3, and 4 identified in ^{69}As, the excited configuration recently observed in ^{67}As [9], and the neutron-aligned band in ^{68}Ge [36]. Unfortunately, positive-parity excited configurations in ^{71,73}As are not known to high enough spin to see the first upbend or backbend, preventing a more detailed systematic comparison. Similar behavior of the $J^{(1)}$ and $J^{(2)}$ in both ^{67,69}As may indicate similar shapes in these nuclei at intermediate spin. The sharp backbendings occurring in all nuclei around 0.53 MeV rotational frequency reflect the change in structures associated in Refs. [9,11,37] with the breaking of a pair of $g_{9/2}$ neutrons, as suggested by the gain of $\sim 7\hbar$ units of angular momentum obtained in each of the alignment processes (see Fig. 7). In ^{68}Ge, additional experimental evidence for the neutron character of the alignment came from the measured g factor of the 8^+ state of the band [38].

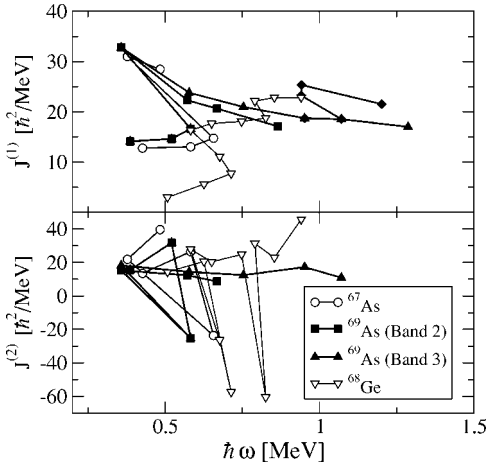

FIG. 6. Kinematic $(J^{(1)})$ and dynamic $(J^{(2)})$ moments of inertia for the excited bands in ^{67,69}As and ^{68}Ge. A value of $K=5/2$ has been used in the analysis. Due to the limited spin range over which band 4 was observed, its dynamic moment of inertia has not been represented.

Above spin $29/2^+$, two modes of rotation are present in ^{69}As, represented by bands 2 and 3 in the level scheme of Fig. 3. Although band 3 is not yrast, it involves a larger intensity of the intraband transitions, suggesting a higher collectivity than in band 2. In Fig. 6 the kinematic and the dynamic moments of inertia for the excited bands in

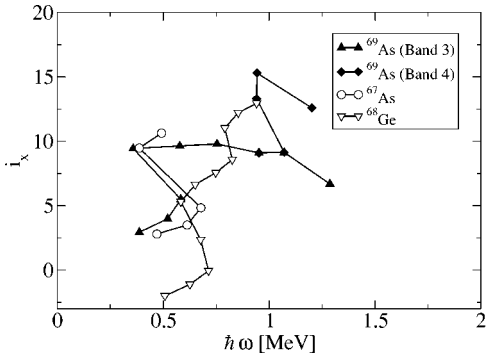

FIG. 7. Alignments $i_x(i_x=I_x-i_{ref})$ in ^{67,69}As and ^{68}Ge. A common set of Harris parameters of $J_0=6\ \hbar^2/\mathrm{MeV}$ and $J_1=3.5\ \hbar^4/\mathrm{MeV}^3$ taken from Ref. [11] has been used for all nuclei. The alignments in the As nuclei have been calculated considering $K=5/2$.

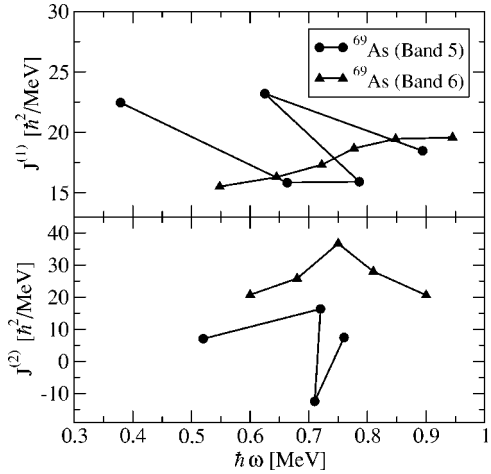

FIG. 8. Kinematic ($J^{(1)}$) and dynamic ($J^{(2)}$) moments of inertia for the $\pi=-$, $\alpha=-1/2$ bands 5 and 6 in ^{69}As. In the plots, the $19/2^-$ states at 4488.7 and 4356.2 keV, respectively, have been taken as the lowest states. A value of $K=5/2$ has been used in the analysis.

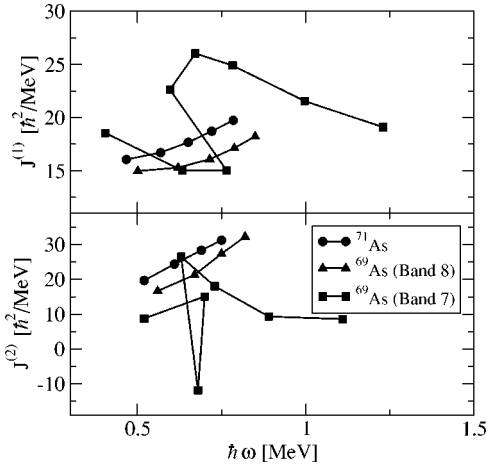

FIG. 9. Kinematic ($J^{(1)}$) and dynamic ($J^{(2)}$) moments of inertia for the $\pi=-$, $\alpha=+1/2$ bands in ^{69,71}As. The $17/2^-$ state at 3844.6 keV has been taken lowest state for both bands. For ^{71}As, the closed circles are the band labeled as band 1 in Ref. [13]. A value of $K=5/2$ has been used in the analysis.

^{69}As, ^{67}As, and ^{68}Ge are plotted. The gradual down sloping of the kinematic moment of inertia of band 3 in ^{69}As at the highest spins is characteristic of a band moving toward termination and losing collectivity. On the contrary, $J^{(1)}$ extracted for the neutron-aligned band in ^{68}Ge increases smoothly. TRS calculations for ^{68}Ge in this spin region predicted two coexisting prolate minima ($\beta_2\approx 0.2$ and $\gamma\approx 13°$; $\gamma\approx -15°$), one being expected to correspond to the band considered in the present work and the other one corresponding to the proton-aligned band [39].

The irregularity in the kinematic moment of inertia at $\hbar\omega\approx 1$ MeV in ^{69}As (see Fig. 6) indicates a second change in the positive-parity yrast line. There, band 4 crosses band 3, the former becoming yrast and contributing to the total alignment with $\sim 6\hbar$ units of angular momentum (Fig. 7).

D. High-spin negative-parity states

The kinematic and the dynamic moments of inertia for the $\pi=-, \alpha=-1/2$ bands 5 and 6 are plotted in Fig. 8. At $\hbar\omega\approx 0.67$ MeV, band 5 undergoes a crossing, as suggested by the very irregular behavior of both $J^{(1)}$ and $J^{(2)}$. Although the kinematic moment of inertia for band 6 shows a smooth increase with increasing rotational frequency, the weak peak around 0.76 MeV in the dynamic moment of inertia may reflect a band crossing also for this structure.

The $\pi=-, \alpha=+1/2$ yrast structure (band 7) exhibits a rather sharp backbending at $\hbar\omega\approx 0.7$ MeV (see Fig. 9) which may be associated with an alignment of $g_{9/2}$ particles in a near-prolate potential. The decrease in $J^{(1)}$ with increasing rotational frequency and the smooth drop in $J^{(2)}$ to values lower than $J^{(1)}$ in band 7 suggests an unpaired regime of rotation typical of terminating bands. On the contrary, both the kinematic and dynamic moments of inertia extracted for band 8 show a smooth increase with increasing rotational frequency. This behavior is similar to that of the $\pi=-, \alpha=+1/2$ yrast band in ^{71}As [12]. In ^{71}As, TRS calculations for rotational frequencies around 0.4 MeV predict a single prolate γ-soft minimum in the potential energy. Above $\hbar\omega=0.6$ MeV this minimum was found to stabilize at $\gamma\approx 30°$ [12].

E. Cranked Nilsson-Strutinsky calculations at high spin

The high-spin states observed in ^{69}As have been compared with the predictions of the cranked Nilsson-Strutinsky (CNS) approach [40]. Within this approach, the observed bands are described in terms of configurations specified by the occupation of the low-j and the high-j valence orbitals with signature α and approximate principal quantum number N [40,41]. The calculated configurations are traced in the deformation space $(\epsilon_2, \epsilon_4, \gamma)$ as a function of spin I. Their energies are usually expressed in terms of $(E-E_{rld})$, i.e., the excitation energies with a rigid rotor reference subtracted [40]. In the present calculations, the $A=80$ parameters given in Ref. [42] have been used for the Nilsson potential. This model neglects the pairing correlations, so the calculations are realistic only for states with spin above $15\hbar$. In the $A\sim 70$ mass region, the CNS model has been rather successful in describing the properties of the high-spin states in ^{68}Ge [36], ^{70}Se [43], and ^{70,72,73}Br nuclei [44–46].

In the following, the configurations calculated for ^{69}As will be specified with respect to the doubly magic $^{56}_{28}Ni_{28}$ core as having five active protons and eight active neutrons. Calculations within the CNS approach for some neighboring nuclei have shown that the properties of the high-spin bands are essentially determined by the number of particles lifted from the $p_{3/2}$, $p_{1/2}$, and $f_{5/2}$ subshells in the $g_{9/2}$ orbitals [36,43–45]. Thus, low-lying configurations in ^{69}As are expected to have one or two $g_{9/2}$ protons and two or three $g_{9/2}$ neutrons.

Those configurations of this type which appear to be relevant when assigning theoretical counterparts to the experimental bands are summarized in Table II. These configura-

TABLE II. The proton and neutron configurations and their contributions to the total configurations drawn in Figs. 10–14. The superscript indicates the number of particles in the different subshells and the subscripts favored total spin contribution from these particles at terminating states. The total configurations, having specified signature and parity (π,α) are labeled by the number of $g_{9/2}$ protons and neutrons with typical γ deformation at intermediate spin as subscript. Furthermore, their terminating spin value is specified and underlined if it coincides with the maximum spin value of that specific configuration, $I_{\max}$. The experimental bands assigned to the different configurations are specified as $B2, B3, \ldots, B8$. Note the specific character of the second neutron configuration where an even number of $f_{5/2}p_{3/2}$ particles couple to an odd-spin value (signature $\alpha=1$) which means that there are two more neutrons of one signature compared with the other signature, in this case four neutrons with $\alpha=+1/2$ and two with $\alpha=-1/2$. It is only in exceptional cases that such configurations come close to yrast and, as discussed in the text, they are only one possible option when considering experimental counterparts in the present case.

Neutrons	Protons		
	$(g_{9/2})^1_{4.5}(f_{5/2}p_{3/2})^4_{4,6}$	$(g_{9/2})^2_8(f_{5/2}p_{3/2})^3_{2.5,4.5}$	$(g_{9/2})^2_8(f_{5/2}p_{3/2})^3_{3.5,5.5}$
$(g_{9/2})^2_8(f_{5/2}p_{3/2})^6_{0,4,6}$	$(+,+1/2)$ $[1,2]_{\gamma\sim30^\circ}, \underline{49/2}^+$ $(B3)$ $[1,2]_{\gamma\sim50^\circ}, \underline{41/2}^+$ $(B2)$	$(-,+1/2)$ $[2,2]_{\gamma\sim15^\circ}, 49/2^-$ $(B7)$ $[2,2]_{\gamma\sim50^\circ}, 41/2^-$	$(-,-1/2)$ $[2,2]_{\gamma\sim15^\circ}, \underline{55/2}^-$ $(B6)$ $[2,2]_{\gamma\sim50^\circ}, \underline{39/2}^-$ $(B5)$
$(g_{9/2})^2_8(f_{5/2}p_{3/2})^6_{3,5}$		$(-,-1/2)$ $[2, 2], 47/2^-$	$(-,+1/2)$ $[2, 2], 45/2^-$
$(g_{9/2})^3_{10.5}(f_{5/2}p_{3/2})^5_{5.5}$	$(-,+1/2)$ $[1, 3], \underline{53/2}^-$ $(B8)$	$(+,+1/2)$ $[2, 3], \underline{57/2}^+$ $(B4)$	
$(g_{9/2})^3_{10.5}(f_{5/2}p_{3/2})^5_{2.5}$	$(-,-1/2)$ $[1, 3], 43/2^-$		

tions are labeled as $[p,n]$ specifying the number of protons (p) and the number of neutrons (n) in the $g_{9/2}$ subshell. The maximum spins of these configurations are in the $I=(25–30)\hbar$ range, as specified in Table II. In the corresponding terminating states at oblate shape, $\gamma=60°$, the deformation is generally rather large, $\varepsilon_2\approx0.30$. At these deformations, the $f_{5/2}$ and $p_{3/2}$ (and $p_{1/2}$) orbitals are generally split apart rather strongly with three $n_z=1$ orbitals with spin projections $m_i=\Omega=\pm5/2$, $\pm3/2$, and $\pm1/2$ coming lowest in energy, as seen in a standard Nilsson diagram; see, e.g., Fig. 1 of Ref. [47]. It is therefore often energetically favorable for the $f_{5/2}p_{3/2}$ valence particles to stay in these low-lying orbitals. For example, with six $f_{5/2}p_{3/2}$ particles, it is favorable for them to couple to $I=0$ or to $I=4$ with one particle lifted to the $n_z=2$ orbitals instead of the maximum spin state $I=6$ when two particles are excited to the $n_z=2$ orbitals. Similarly, with five $f_{5/2}p_{3/2}$ particles having signature $\alpha=+1/2$, it is more favorable for them to couple to $I=5/2$ than the maximal spin state $I=9/2$. These facts are reflected in the proton and neutron configurations listed in Table II.

Combining the proton and neutron configurations of Table II leads to total configurations which terminate at their maximal spin values as well as configurations which terminate at lower spin. These different configurations often lead to coexistent minima in the potential energy surfaces with γ deformations at intermediate spin in the range 15°–30° for the former and $\gamma\approx50°$ for the latter. Thus, they are labeled with such an approximate γ value in Table II.

In the top panel of Fig. 10, the $(E-E_{rld})$ curves for the lowest calculated $\pi=+,\alpha=+1/2$ bands are shown. At low spin, a configuration with one proton and two neutrons in the $g_{9/2}$ orbital ([1, 2]) is calculated to be lowest in energy. This configuration was found to exhibit two minima in the potential energy surface, one at $\gamma\approx50°$ and the other at $\gamma\approx30°$, see Fig. 11. The bands $[1,2]_{\gamma\sim50°}$ and $[1,2]_{\gamma\sim30°}$ are built on these minima. The [2, 3] configuration lies somewhat higher at low spins but falls rapidly with increasing spin and is predicted to cross the configuration $[1,2]_{\gamma\sim30°}$ at spin $41/2^+$.

These calculated configurations are compared with those of the experimental positive-parity bands 2, 3, and 4. Con-

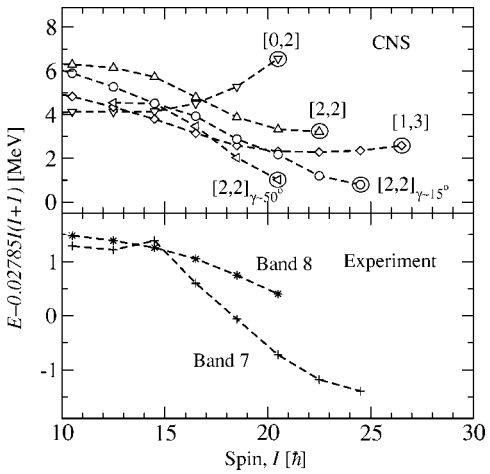

FIG. 10. Calculated (top) and experimental (bottom) energies of the $(\pi=+,\ \alpha=+1/2)$ configurations relative to a standard rotor reference. The calculated bands are labeled by the number of the $g_{9/2}$ protons and neutrons. The aligned states $(\gamma=60°)$ are indicated by large open circles. The maximum spin for the $[1,2]_{\gamma\sim30°}$ configuration is predicted at $\gamma\sim53°$, which can in principle be considered a terminating state.

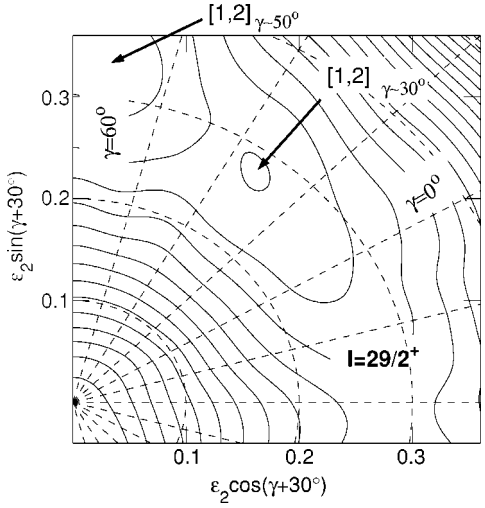

FIG. 11. Potential-energy surface for the $(\pi=+, \alpha=+1/2)$, [1,2] configuration at spin $I=29/2^+$. The minima are located at $\varepsilon_2 \approx 0.33$, $\gamma \approx 50°$ and $\varepsilon_2 \approx 0.28$, $\gamma \approx 30°$. The energy difference between neighboring equipotential lines is 0.4 MeV.

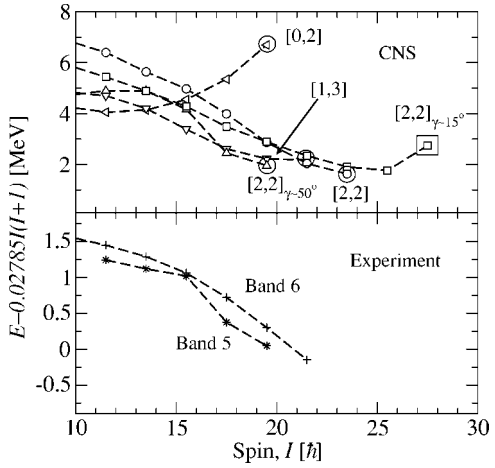

FIG. 12. Same as Fig. 10 but for negative-parity bands with signature $\alpha=-1/2$. The open square indicates a collective state of maximum spin, $I_{\max}$.

figurations $[1,2]_{\gamma\sim 50°}$ and $[1,2]_{\gamma\sim 30°}$ are good candidates for bands 2 and 3, respectively. The experimental and the calculated bands show about the same curvature in the energy graphs. The calculated terminating spins for the $[1,2]_{\gamma\sim 50°}$ and $[1,2]_{\gamma\sim 30°}$ configurations (see Table II and Fig. 3) suggest that these bands are observed up to two units of angular momentum below their respective terminations. The crossing between the two experimental bands, observed around spin $29/2^+$ is not well described by the theory. However, the exact crossing point is sensitive to the detailed features of the single-particle energies used in the model. Moreover, in this spin region pairing correlations could still be important so the CNS calculations should be considered with some caution.

In the spin range $45/2^+$–$57/2^+$, the [2,3] configuration is calculated to be the lowest in energy. This is in close agreement with the experimental situation where at spin $45/2^+$, band 4 becomes yrast (Fig. 10, bottom). Thus, the crossing between band 3 and band 4 may be interpreted as the crossing between configurations with different numbers of $g_{9/2}$ particles ([1,2] and [2,3], respectively) and slightly different deformations. At the predicted crossing spin $I=41/2^+$, the calculated shapes for the $[1,2]_{\gamma\sim 30°}$ and [2,3] configurations are $\varepsilon_2=0.24$, $\gamma=22°$ and $\varepsilon_2=0.33, \gamma=26°$, respectively. In this region of rather high rotational frequencies, it is reasonable to believe that at crossing, the $g_{9/2}$ particles in the [2, 3] configuration have their angular momentum almost fully aligned with the axis of rotation. A gain in alignment of $\sim 6\hbar$ units is expected from the additional $g_{9/2}$ proton and neutron in the [2, 3] configuration with respect to the $[1,2]_{\gamma\sim 30°}$ configuration. This is in a very good agreement with the experimental observations (see Fig. 7).

In this spin region, the TRS calculations for ^{69}As performed in Ref. [11] predicted a strongly deformed minimum $(\beta_2 \approx 0.45)$ coexisting with a triaxial prolate minimum $(\beta_2 \approx 0.20, \gamma \approx 25°)$. The corresponding configuration has one or two protons excited from the $f_{7/2}$ orbitals. Evidence for a superdeformed band obtained by promoting two protons from the $f_{7/2}$ orbital into the $g_{9/2}$ orbital has been reported in the neighboring even-even core ^{68}Ge and interpreted within the CNS approach [36]. The experimental excitation energy of the band is not known so the calculated configurations with two proton holes in the $f_{7/2}$ subshell were compared with the superdeformed band in ^{68}Ge assuming different spin values and arbitrary excitation energies [36]. The nucleus ^{69}As is only one proton away from ^{68}Ge, so, in principle, a $f_{7/2}^{-2}$ strongly deformed band is likely to occur, although it is not expected to become yrast until very high spin. We have carried out calculations for a few low-lying configurations of this kind and we found that they are predicted to lie 1–2 MeV higher in energy than the lowest pure valence space configurations. On the other hand, they become yrast around $I=30\hbar$ when the spin is exhausted in the valence space configurations.

The lowest calculated $\pi=-, \alpha=-1/2$ configurations are represented in the top panel of Fig. 12. Above spin $15\hbar$, four configurations are predicted to lie close to the yrast line, all of which being energetically favored at some spin. The calculations indicate that the [1, 3] configuration competes with three configurations of [2,2] nature in the $31/2^-$–$43/2^-$ spin range. Configurations $[2,2]_{\gamma\sim 50°}$ and $[2,2]_{\gamma\sim 15°}$ are built in the two competing minima in the potential energy surface of the same fixed configuration, which differ from the configuration simply labeled as [2,2] by the signature of the (fp) particles (see Fig. 13 and Table II).

The [1,3] and $[2,2]_{\gamma\sim 50°}$ configurations (or some mixture of them) are both candidates for band 5, above spin $31/2^-$ (Fig. 12, lower panel). The theoretical band [1,3] is calculated to terminate at spin $43/2^-$, whereas the termination for the band $[2,2]_{\gamma\sim 50°}$ is reached at spin $39/2^-$.

When drawn relative to a rigid rotor reference, the energy graph of the $\pi=-, \alpha=-1/2$ band 6 decreases smoothly with increasing spin as illustrated in the lower panel of Fig. 12. This behavior is similar to that of the calculated bands [2,2] and $[2,2]_{\gamma\sim 15°}$. Since below spin $39/2^-$, $[2,2]_{\gamma\sim 15°}$ is lower in energy than [2,2], the former is favored in the interpreta-

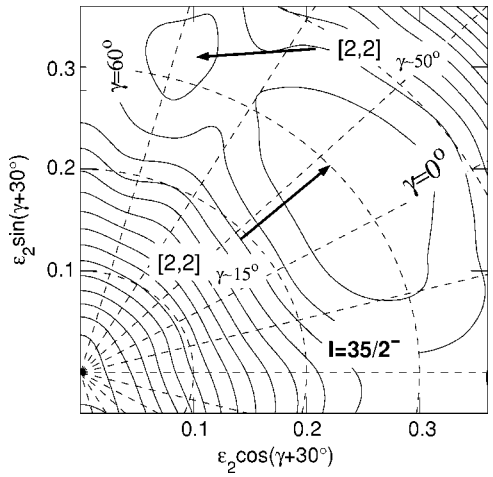

FIG. 13. Potential-energy surface for the $(\pi=-,\alpha=-1/2)$, [2,2] configuration at spin $I=35/2^-$. The minima are located at $\varepsilon_2 \approx 0.31$, $\gamma \approx 50°$ and $\varepsilon_2 \approx 0.3$, $\gamma \approx 15°$. The energy difference between neighboring equipotential lines is 0.4 MeV.

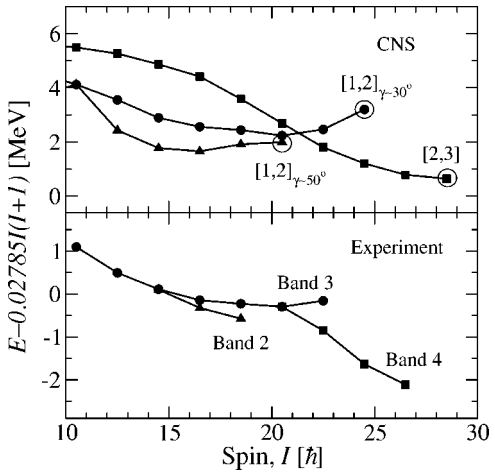

FIG. 14. Same as Figs. 10 and 12 but for negative-parity bands with signature $\alpha=+1/2$.

tion of the experimental band 6. Furthermore, at spin $31/2^-$, the two minima corresponding to the $[2,2]_{\gamma\sim50°}$ and $[2,2]_{\gamma\sim15°}$ configurations are predicted very close in energy, in agreement with the observed near-degeneracy of bands 5 and 6. Due to the similar structures of these two configurations and the rather small potential-energy barrier between them, it is expected that they will mix strongly. Such mixing may be the cause for the irregularities observed in the dynamic moments of inertia of the two bands, as discussed in the previous section (see also Fig. 8). This situation is similar to that recently found in the even-even neighboring nucleus ^{70}Se [43]. There, the potential-energy surface calculated for the $\pi=-,\alpha=-1/2$ structures showed two minima that developed from configurations with the same number of nucleons lifted from the fp shell to the $g_{9/2}$ orbital. The two observed negative-parity bands were believed to belong to such different minima, thus representing a coexistence of different nuclear shapes at high spin [43].

For the last two states observed in band 6, our calculations predict a crossing of the $[2,2]_{\gamma\sim15°}$ and [2,2] configurations. The latter becomes lowest after the crossing but the two configurations remain close in energy. In any case, the question arises whether the high-spin part of the [2,2] configuration should rather be considered when making configuration assignments to the experimental band 6. In fact, the relative energies and the crossings of the calculated bands depend on the parametrization of the Nilsson potential. In order to investigate this effect, we have also carried out calculations using the set of single-particle parameters from Ref. [47]. Employing this set of parameters, we found that the configurations discussed above do not exhibit any crossing, they only come very close in energy in the spin region of interest.

The lowest calculated $\pi=-$, $\alpha=+1/2$ configurations are displayed in the top panel of Fig. 14. The positive signature of the theoretical bands is obtained by changing the signature of an (fp) neutron in the [1,3] configuration and the signature of an (fp) proton in all other configurations, with respect to their negative signature partners discussed above. From the comparison of the theoretical $(E-E_{rld})$ curves with that of band 7 (Fig. 14) it is clear that band 7 cannot be identified with the band $[2,2]_{\gamma\sim50°}$, because this configuration is predicted to terminate below the maximum spin observed in band 7. The theoretical band is built in the noncollective minimum of the potential energy surface displayed in Fig. 15 and may not have a counterpart in the observed spectrum. The next lowest calculated configuration which might be taken into account in the interpretation of band 7 is the [1,3] configuration. However, we prefer to associate band 7 with the configuration $[2,2]_{\gamma\sim15°}$ because of the better agreement in the slopes of the corresponding energy graphs above spin $29/2^-$. The calculated termination for the $[2,2]_{\gamma\sim15°}$ configuration at spin $49/2^-$ coincides with the maximum spin observed in band 7, this suggesting that this band has been observed to termination.

The correspondence between the slopes of the theoretical and experimental $(E-E_{rld})$ curves suggests that the configu-

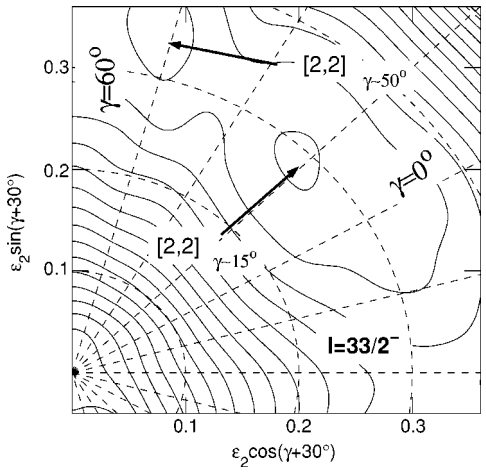

FIG. 15. Potential-energy surface for the $(\pi=-,\alpha=+1/2)$, [2,2] configuration at spin $I=33/2^-$. The minima are located at $\varepsilon_2 \approx 0.31$, $\gamma \approx 50°$ and $\varepsilon_2 \approx 0.29$, $\gamma \approx 15°$. The energy difference between neighboring equipotential lines is 0.4 MeV.

rations [1,3] and [2,2] may be considered when making assignments for band 8. For this band, however, more experimental information at higher spin than that observed in the present work is needed in order to make a more firm assignment.

V. SUMMARY

We have revised and extended the previously known level scheme of the nucleus ^{69}As, employing the ^{40}Ca(^{32}S,3p) reaction. Double and triple γ-ray coincidences and directional correlations have been measured. The present analysis brings a large amount of new information about the structure of ^{69}As at high spin. The previously observed positive-parity band has been extended up to spin $(53/2^+)$. The continuation of the ground state band has also been investigated up to spin $(29/2^+)$. Three negative-parity bands have been observed for the first time, and the negative-parity band identified in [10] has been extended up to spin $(49/2^-)$. It was found that, at low spin, the negative-parity bands coexist with states of single-particle character suggesting a competition of shapes with different deformations. No experimental evidence for a $f_{7/2}$ proton-hole low-lying negative-parity band could be found, which may indicate that in this energy region ^{69}As is less deformed than ^{71}As.

The high-spin bands were interpreted using the cranked Nilsson-Strutinsky formalism. It was shown that their properties are essentially determined by the number of the nucleons lifted from the fp shell to the $g_{9/2}$ orbital. The crossing of the positive-parity bands 3 and 4 was interpreted as being the crossing of $\pi(g_{9/2})^1\nu(g_{9/2})^2$ (band 3) and $\pi(g_{9/2})^2\nu(g_{9/2})^3$ (band 4) configurations with slightly different deformations. The theoretical bands are predicted to terminate at spins $49/2^+$ and $57/2^+$, respectively, in each case two units of angular momentum higher than the maximum spin experimentally observed. Configurations of $\pi(g_{9/2})^2\nu(g_{9/2})^2$ and $\pi(g_{9/2})^1\nu(g_{9/2})^3$ nature were proposed for the negative-parity bands, the theory predicting that one band was observed to termination and the other bands to spin values close to their respective terminations.

ACKNOWLEDGMENTS

The authors wish to thank Professor A. Gelberg for useful discussions. A.J. acknowledges financial support from the Spanish Ministerio de Ciencias y Tecnologia within the program "Ramón y Cajal." The authors thank the crew of the VIVITRON accelerator for their efficient support during the experiments. This work was supported by BMBF under Contracts No. 06 OK 958, No. O6 K167, and No. 06 GÖ 951, the EUROVIV Contract No. HPRI-CT-1999-000783, Swedish Science Research Council and European Community under TMR Contract No. ERBFMRX CT97-0123.

[1] U. von Hundelshausen, Z. Phys. **225**, 125 (1969).
[2] Ph. Dessagne *et al.*, Phys. Rev. C **37**, 2687 (1988).
[3] R. R. Betts, D. J. Pullen, W. Scholz, and B. Rosner, Phys. Rev. Lett. **26**, 1576 (1971).
[4] P. van der Merwe, E. Barnard, J. A. M de Villiers, and J. G. Malan, Nucl. Phys. **A240**, 273 (1975).
[5] B. Heits *et al.*, Phys. Lett. **61B**, 33 (1976).
[6] B. Heits *et al.*, Phys. Rev. C **15**, 1742 (1977).
[7] H. P. Hellmeister *et al.*, Phys. Rev. C **17**, 2113 (1978).
[8] T. F. Lang *et al.*, Phys. Rev. C **42**, R1175 (1990).
[9] D. G. Jenkins *et al.*, Phys. Rev. C **64**, 064311 (2001).
[10] S. Mitarai *et al.*, JAERI Rev. **97-010**, 23 (1997).
[11] A. M. Bruce *et al.*, Phys. Rev. C **62**, 027303 (2000).
[12] R. S. Zighelboim *et al.*, Phys. Rev. C **50**, 716 (1994).
[13] N. Fotiades *et al.*, Phys. Rev. C **59**, 2919 (1999).
[14] F. A. Beck, Prog. Part. Nucl. Phys. **28**, 443 (1992).
[15] J. Simpson, Z. Phys. A **358**, 39 (1997).
[16] J. Eberth *et al.*, Prog. Part. Nucl. Phys. **28**, 495 (1992).
[17] G. Duchêne *et al.*, Nucl. Instrum. Methods Phys. Res. A **432**, 90 (1999).
[18] A. Gadea *et al.*, LNL Annual Report No. 160/00, 1999, p. 151.
[19] Ö. Skeppstedt *et al.*, Nucl. Instrum. Methods Phys. Res. A **421**, 531 (1999).
[20] D. Bazzacco, GASP Data Analysis Program Package, 1997.
[21] D. C. Radford, Nucl. Instrum. Methods Phys. Res. A **361**, 297 (1995).
[22] A. Krämer-Flecken *et al.*, Nucl. Instrum. Methods Phys. Res. A **275**, 333 (1989).
[23] H. A. Helms, W. Hogervorst, G. J. Zaal, and J. Blok, Phys. Scr. **14**, 138 (1976).
[24] F. J. Bergmeister, A. Henriquez Frings, A. Gelberg, and K. P. Lieb, Z. Phys. A **296**, 181 (1980).
[25] V. Zobel, L. Cleemann, J. Eberth, T. Heck, and W. Neumann, Nucl. Phys. **A346**, 510 (1980).
[26] F. Becker *et al.*, Nucl. Phys. **A626**, 799 (1997).
[27] U. Hermkens *et al.*, Phys. Rev. C **52**, 1783 (1995).
[28] E. Nolte, Y. Shida, W. Kutschera, R. Prestele, and H. Morinaga, Z. Phys. **268**, 267 (1974).
[29] W. Scholz and F. B. Malik, Phys. Rev. **176**, 1355 (1968).
[30] H. Toki and A. Faessler, Nucl. Phys. **A253**, 231 (1975).
[31] H. Toki and A. Faessler, Phys. Lett. **63B**, 121 (1976).
[32] D. Sohler *et al.*, Nucl. Phys. **A618**, 35 (1997).
[33] S. E. Larsson, G. Leander, and I. Ragnarsson, Nucl. Phys. **A307**, 189 (1978).
[34] I. Ragnarsson *et al.*, Hyperfine Interact. **43**, 425 (1988).
[35] A. P de Lima *et al.*, Phys. Rev. C **23**, 213 (1981).
[36] D. Ward *et al.*, Phys. Rev. C **63**, 014301 (2000).

[37] U. Hermkens *et al.*, Z. Phys. A **343**, 371 (1992).
[38] M. E. Barclay *et al.*, J. Phys. G **12**, L295 (1986).
[39] E. Stefanova *et al.*, Phys. Rev. C **67**, 054319 (2003).
[40] A. V. Afanasjev, D. B. Fossan, G. J. Lane, and I. Ragnarsson, Phys. Rep. **322**, 1 (1999).
[41] A. V. Afanasjev and I. Ragnarsson, Nucl. Phys. **A591**, 387 (1995).
[42] D. Galeriu, D. Bucurescu, and M. Ivascu, J. Phys. G **12**, 329 (1986).
[43] G. Rainovksi *et al.*, J. Phys. G **28**, 2617 (2002).
[44] D. G. Jenkins *et al.*, Phys. Rev. C **65**, 064307 (2002).
[45] C. Plettner *et al.*, Phys. Rev. Lett. **85**, 2454 (2000).
[46] C. Plettner *et al.*, Phys. Rev. C **62**, 014313 (2000).
[47] T. Bengtsson and I. Ragnarsson, Nucl. Phys. **A436**, 14 (1985).